




## Article

# Elevated Temperature Tribological Behavior of Duplex Layer CrN/DLC and Nano Multilayer DLC-W Coatings Deposited on Carburized and Hardened 16MnCr5 Steel

Funsho Olaitan Kolawole <sup>1</sup>, Shola Kolade Kolawole <sup>2</sup>, Newton Kiyoshi Fukumasu <sup>3</sup>, Luis Bernardo Varela <sup>1</sup>, Paulo Konrad Vencovsky <sup>4</sup>, Danilo Assad Ludewigs <sup>4</sup>, Roberto Martins de Souza <sup>3</sup>, and André Paulo Tschiptschin <sup>1,\*</sup>

<sup>1</sup> Metallurgical and Materials Engineering Department, University of São Paulo, São Paulo 05508-030, Brazil; fkopresido@yahoo.com (F.O.K.); luisvarelajimenez@alumni.usp.br (L.B.V.)

<sup>2</sup> National Agency for Science and Engineering Infrastructure, Abuja 900106, Nigeria

<sup>3</sup> Surface Phenomena Laboratory, Polytechnic School of the University of São Paulo, São Paulo 05508-030, Brazil; newton.fukumasu@gmail.com (N.K.F.); robertosouza@usp.br (R.M.d.S.)

<sup>4</sup> HEF Durferit do Brasil Química LTDA, R. 27 de Março, 91-Canhema, Diadema 00941-450, Brazil; pvencovsky@hef.group (P.K.V.); dludewigs@hef.group (D.A.L.)

\* Correspondence: antschip@usp.br

**Abstract:** This study investigates the impact of temperature on the tribological performance of duplex layer CrN/DLC and nano-multilayers DLC-W coatings deposited using hybrid PVD-PECVD techniques on carburized and hardened 16MnCr5 discs cut from internal combustion engines valve tappets. Reciprocating dry sliding experiments were conducted at 25 °C, 150 °C, 200 °C, and 250 °C to analyze the high-temperature tribological behavior of the coatings. The wear mechanisms were characterized using SEM, EDS mapping, Raman spectroscopy, and nanoindentation. The lowest coefficient of friction was obtained for CrN/DLC at 25 °C. The CrN/DLC coefficients of friction (COF) increase with temperatures due to increasing adhesive wear. Similarly, DLC-W exhibited a comparable trend with increasing temperature from 25 °C to 250 °C. Both coatings' wear resistance decreased with higher temperatures due to the transformation of sp<sup>3</sup> C bonds to sp<sup>2</sup> C bonds, facilitating the plastic deformation of the coatings and afterward of the substrate. The CrN/DLC displayed superior wear resistance to the DLC-W coating across all temperatures. The DLC-W multilayer coating showed poor wear resistance above 150 °C, being completely removed during the testing. Compared to both coatings, the uncoated 16MnCr5 discs exhibited higher coefficients of friction and wear rates at all temperatures. Predominant wear mechanisms observed in the coated discs were adhesive and abrasive. The study revealed a decrease in the coatings' structural and mechanical properties with rising temperatures. Hard abrasive WC particles were identified as contributing to increased wear rates in the multilayer DLC-W coatings.

**Keywords:** adhesion; CrN/DLC; DLC-W; wear mechanisms; tribological behavior; elevated temperature



**Citation:** Kolawole, F.O.; Kolawole, S.K.; Fukumasu, N.K.; Varela, L.B.; Vencovsky, P.K.; Ludewigs, D.A.; de Souza, R.M.; Tschiptschin, A.P. Elevated Temperature Tribological Behavior of Duplex Layer CrN/DLC and Nano Multilayer DLC-W Coatings Deposited on Carburized and Hardened 16MnCr5 Steel. *Coatings* **2024**, *14*, 1197. <https://doi.org/10.3390/coatings14091197>

Academic Editor: Csaba Balázs

Received: 19 August 2024

Revised: 11 September 2024

Accepted: 12 September 2024

Published: 17 September 2024



**Copyright:** © 2024 by the authors. Licensee MDPI, Basel, Switzerland. This article is an open access article distributed under the terms and conditions of the Creative Commons Attribution (CC BY) license (<https://creativecommons.org/licenses/by/4.0/>).

## 1. Introduction

The demand for protective coatings with superior wear resistance and durability for automobile combustion engines operating at high temperatures (100–200 °C) is growing, particularly in racing cars [1–3]. Diamond-like carbon (DLC) coatings have been employed in such applications owing to their environmentally friendly characteristics, inert nature, ultra-low friction, and exceptional mechanical properties (high hardness and elastic modulus). These coatings also exhibit excellent tribological behavior, particularly in wear and friction, at temperatures above room temperature [1,3–5]. DLC coatings are known for withstanding tribological stresses at temperatures up to 300 °C. However, the tribological behavior of these coatings at intermediate temperatures below 300 °C is lacking. Challenges

also arise when applying DLC coatings to automobile components made of materials such as steel, aluminum, cast iron, or other metals. This is primarily due to the low adhesion between the substrate and the DLC coatings [5]. Consequently, this issue increases delamination, micro-pitting, micro-abrasion, elevated friction, reduced wear resistance, and oxidation at higher temperatures (100–200 °C) [5–7].

Enhancing the adhesion properties of DLC coatings is achieved by applying adhesive interlayers and doping with different metals or non-metals during deposition. This procedure solves challenges associated with DLC's high-temperature tribological behavior [8,9]. The tribological performance is significantly influenced by intrinsic hydrogen content, doping elements, and the  $sp^2/sp^3$  ratio [10,11]. Interlayers such as Si, SiH, Cr, or CrN have demonstrated efficacy in improving the adhesion between coatings and metallic substrates [12–15]. Similarly, introducing metallic dopants like W, Mo, Ti, or Si has been proven to enhance the adhesion of DLC to metallic substrates [5]. These interlayers and metallic dopants contribute to increased surface energies, improved interfacial fracture toughness, and reduced internal stress by strengthening the bond layer of the coatings. The reduction in wear rates and coefficients of friction creates a transfer layer on the counter surface that forms a tribofilm under wet and dry conditions [16,17].

Various deposition techniques, including Chemical Vapour Deposition (CVD), Plasma Enhanced Chemical Vapor Deposition (PECVD), Magnetron Sputtering, Plasma Source Ion Deposition, and Direct Current/Radio Frequency Sputtering, have been employed for the deposition of CrN/DLC coatings. On the other hand, DLC-W multilayer coatings have been deposited by different hybrid processes involving PVD techniques, Direct Current Magnetron Sputtering (DCMS), High Power Impulse Magnetron Sputtering (DCMS-HiPIMS), combined with Radio-Frequency Plasma Enhanced Chemical Vapor Deposition, Direct-Current Plasma Enhanced Chemical Vapor Deposition (DC-PECVD), and Ion Beam Assisted Deposition (IBAD) [18–22].

Hybrid combinations of these deposition methods will likely produce CrN/DLC and DLC-W coatings with excellent mechanical and tribological behavior. Few studies have been reported about the tribological behavior of these coatings at intermediate temperatures below 300 °C. This research aims to characterize and understand the tribological behavior of CrN/DLC and DLC-W coatings at temperatures below 300 °C. Tribological tests of CrN/DLC and DLC-W coated discs at 25 °C, 150 °C, 200 °C, and 250 °C were carried out. The CrN/DLC and DLC-W coatings were deposited on carburized and hardened 16MnCr5 steel discs using hybrid Physical Vapour Deposition (PVD) and Plasma Enhanced Chemical Vapour Deposition (PECVD) above room temperature. The high-temperature tribological behavior of CrN/DLC and DLC-W from 25 °C to 250 °C was studied using SRV linear reciprocating equipment [Schwingung (Oscillating), Reibung (Friction), Verschleiß (Wear)]. The operative wear mechanisms inside and outside the worn surface are discussed based on microstructural and chemical characterizations carried out by SEM, EDS mapping, Raman analysis, and nanoindentation measurements to observe structural and mechanical properties changes.

## 2. Materials and Methods

Carburized and hardened 16MnCr5 steel discs were cut from 6 sets of Ford Ka 1.0 mechanical valve tappets 21 mm in height and 25 mm in diameter. A total of 36 flat discs 25 mm in diameter and 3 mm in height served as substrates for depositing the two types of coatings: CrN/DLC and DLC-W. The surface hardness of the carburized discs was 929 HV0.1.

### 2.1. Coating Deposition

The coatings were deposited on the flat surface of the carburized and hardened 16MnCr5 steel discs.

The nominal chemical composition of the valve tappets is C— (0.14%–0.19%), Mn— (1.05%–1.30%), Si— (0.4% max), Cr— (0.85%–1.10%), P— (0.025% max), S— (0.035%) and Fe (balance). After carburizing, the surface of the tappets attained 0.8 wt.% C.

The carburized and hardened 16MnCr5 steel discs were then polished to obtain an average surface roughness ( $R_a$ ) of 0.05  $\mu\text{m}$ . After that, the discs were ultrasonically cleaned in ethanol and acetone for 20 min. A hybrid Physical Vapour Deposition (PVD)–Plasma Enhanced Chemical Vapour Deposition (PECVD) reactor was then used to deposit the CrN/DLC and DLC-W coatings. The chamber temperature was 180  $^{\circ}\text{C}$ , and the pressure was  $2.5 \times 10^{-6}$  mbar which were kept constant for 120 min. During the CrN/DLC deposition, plasma etching was allowed for 10 min, followed by a Cr adhesion interlayer deposition for 5 min using a Cr target. A CrN layer was deposited afterward, using a Cr target (99.99% purity) and  $\text{N}_2$  gas for 60 min. Lastly, the DLC layer was deposited using  $\text{C}_2\text{H}_2$  gas for 60 min for the CrN/DLC coating.

The DLC-W coating started with plasma etching of the substrate for 40 min, followed by a WC adhesion interlayer deposition using a WC target (99.99% purity) for 5 min. Finally, the DLC-W coating was deposited using the same WC target and  $\text{C}_2\text{H}_2$  gas for 180 min. The deposition parameters used for the production of the two coatings, the chemical compositions, and the coating properties are summarized in Table 1.

**Table 1.** Coating’s designation, deposition parameters, chemical composition, and main properties of CrN/DLC and DLC-W.

Sample Designation	CrN/DLC	DLC-W
Power applied on CrN deposition	15,000 W	
Power applied on microwave Guns	3000 W	
Power applied on sputtering		17,000 W
Plasma etching	substrate bias 150 V, 150 kHz, and Airflow 100 sccm	substrate bias 150 V, 150 kHz, and Airflow 110 sccm
Frequency	150 kHz	150 kHz
Air flow rate	110 sccm	300 sccm
$\text{N}_2$ flow rate	300 sccm	
$\text{C}_2\text{H}_2$ flow rate	1400	600
Bias	Cr/CrN—150 V DLC—330 V Cr—0.35 $\mu\text{m}$	WC—150 DLC-W—100
Coating thickness	CrN—0.75 $\mu\text{m}$ DLC—1.85 $\mu\text{m}$ C—97 (at. %) Cr—2.5 (at. %) N—0.5 (at. %) O—1 (at. %)	WC—0.58 $\mu\text{m}$ DLC-W—6 $\mu\text{m}$ C—31 (at. %) W—65 (at. %) O—4 (at. %)
Chemical composition (at. %)		
Hardness	$18.85 \pm 0.42$ GPa	$9.88 \pm 1.76$ GPa
Elastic modulus	$154.93 \pm 3.21$ GPa	$101.94 \pm 8.13$ GPa
Elastic strain to failure—H/E	$0.122 \pm 0.001$	$0.097 \pm 0.005$
Plastic deformation— $\text{H}^3/\text{E}^2$	$0.279 \pm 0.001$ GPa	$0.093 \pm 0.002$ GPa
Elastic recovery	71.04 %	67.12 %

## 2.2. Coatings Characterization

The as-deposited CrN/DLC and DLC-W coatings’ surface topography was obtained using a Bruker, multimode 8, Atomic Force Microscope (AFM), with a silicon nitride tip of  $k \sim 0.5$  N/m. The scan size used for roughness measurements was 20  $\mu\text{m}$  in the contact mode. The mechanical properties (hardness and Young modulus) were measured using a Hysitron TI 950 nanoindenter, a diamond Berkovich pyramid, a 10 mN load, and load and unload rates of 5 mN/min. The indentation depth was less than 10% of the film thickness to minimize a substrate effect. The structure of the coatings was analyzed using Raman spectroscopy (confocal Horiba® Xplora One™) having a 532 nm excitation wavelength laser source, with an 1800 grating per mm diffraction mesh, a 50  $\mu\text{m}$  slit, and a

100× objective lens. Raman spectra in regions up to 1 µm in diameter were acquired. The spectral resolution was 2 cm<sup>-1</sup>, and the scan range was 400 to 2400 cm<sup>-1</sup>. Origin v9.5 software was used to process all acquired Raman spectra, using a Gaussian non-linear curve fit with an R<sup>2</sup> higher than 0.95 to deconvolute the D and G shift positions. The ratio ID/IG was considered an indicator of the carbon sp<sup>2</sup>/sp<sup>3</sup> structure. Full details on the characterization of the coatings have been reported in our previous work [23].

### 2.3. Reciprocating Wear Test

Tribological tests were carried out in an Optimol SRV<sup>®</sup> v4 device with a ball on-plane configuration under a dry condition in a reciprocating slide (Figure 1). Tests were carried out under a load of 20 N for 30 min, 10 Hz of Reciprocating frequency and a stroke of 2 mm at 25 °C, 150 °C, 200 °C, and 250 °C. 60 HRC AISI 52,100 steel spheres were used as contact bodies. The load condition corresponds to an initial Hertzian contact pressure of 970–1154 MPa and a maximum shear stress of 289–358 MPa. The COF for both coatings was recorded during the experiment. The reciprocating tests were conducted in triplicate for each test condition for repeatability.

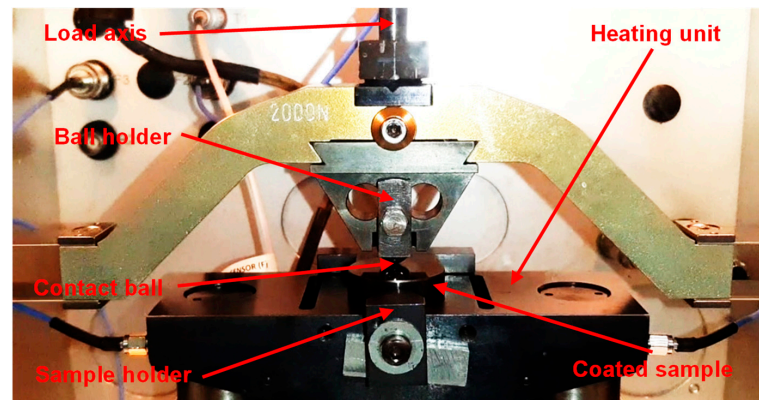


**Figure 1.** Scheme of the Reciprocating Optimol SRV tribometer.

### 2.4. Wear Analysis

The wear tracks and wear scars of the uncoated and coated discs were observed by SEM. Energy-dispersive X-ray spectroscopy (EDS) was used to analyze the wear tracks' chemical composition, obtaining EDS elemental mapping images from the wear track. The wear volumes were measured using the 3D coherence correlation interferometry technique (CCI) in a Taylor Hobson profilometer. The structure and mechanical properties inside the wear track were evaluated using Raman spectroscopy and nanoindentation, respectively. The specific wear rate ( $W_s$ ) of the uncoated, CrN/DLC, and DLC-W coated discs tested at 25 °C, 150 °C, 200 °C, and 250 °C were calculated using Equation (1):

$$W_s = \frac{\Delta V}{(F_n \cdot S)} \quad (1)$$

$\Delta V$  being the wear volume,  $F_n$  the normal load, and  $S$  the sliding distance.

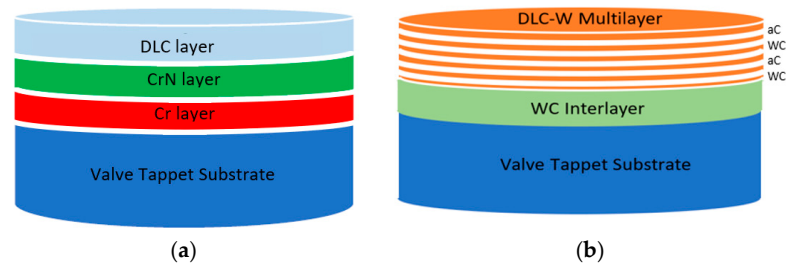
## 3. Results and Discussion

The CrN/DLC and DLC-W coatings were successfully grown by PVD/PECVD. The CrN/DLC coating has a duplex layer coating architecture, with an underlying 0.35 µm thick Cr adhesive layer, followed by a 0.75 µm CrN reinforcing layer and finally, a 1.85 µm thick DLC layer, with a total thickness of 2.95 µm. The DLC-W coating is preceded by a WC adhesion interlayer 0.58 µm in thickness. The DLC-W coating shows a multilayer columnar structure with a 6.58 µm total thickness.

The structural properties and composition of the DLC films were determined by Raman spectroscopy. The D and G positions for CrN/DLC were 1375.73 cm<sup>-1</sup> and



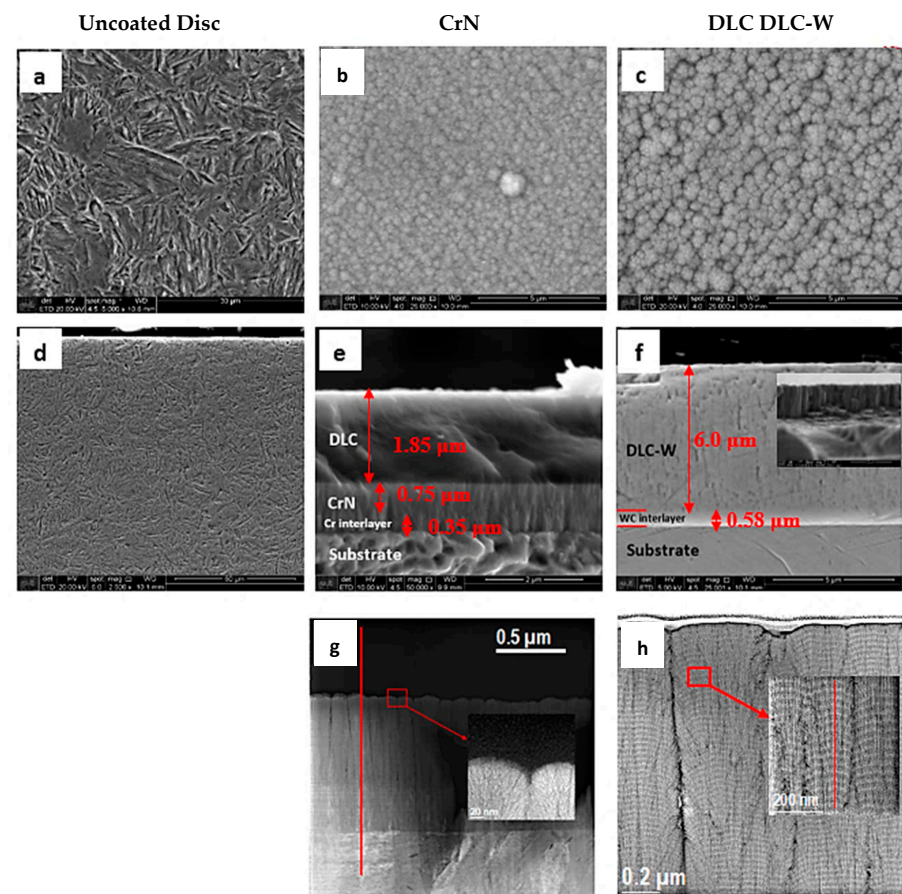
1544.13  $\text{cm}^{-1}$ , respectively, while the D and G positions for DLC-W were 1368.05  $\text{cm}^{-1}$  and 1546.53  $\text{cm}^{-1}$ , respectively. The ID/IG ratios were 0.84 and 1.69 for CrN/DLC and DLC-W, respectively. The results indicate a higher  $\text{sp}^3$  bonding for CrN/DLC than DLC-W. Adding tungsten to the DLC favors the formation of  $\text{sp}^2$ -bonded carbon sites in the amorphous DLC matrix. Figure 2a,b schematically show the architecture of both coatings.



**Figure 2.** Architecture of the (a) CrN-DLC coating and (b) the DLC-W multilayer coating.

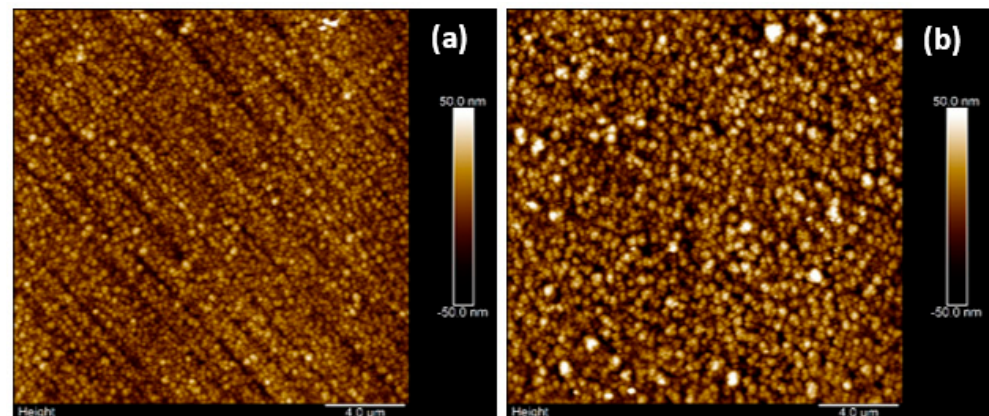
While the CrN-DLC consists of a monolithic DLC layer deposited on top of a CrN reinforcing layer, the DLC-W multilayer consists of alternate amorphous carbon and WC-rich amorphous layers.

Figure 3a–h shows images of the microstructure of the coatings. The top surface images Figure 3a–c show cauliflower structures on top of the CrN/DLC and the DLC-W films; the DLC-W coating shows a coarser structure than the CrN/DLC, with a greater roughness. The cross-section images Figure 3d–f shows the columnar structure and thicknesses of the reinforced CrN/DLC and the DLC-W coatings. The TEM images show the columnar growth of both coatings and the nanostructured multilayered DLC-W coating.



**Figure 3.** Microstructure of the coatings: (a–c) Top surface SEM images; (d–f) cross-section SEM images; (g,h) cross-section TEM images.

Figure 4a,b presents the AFM images of the CrN/DLC and DLC-W coated discs for surface topography. The CrN/DLC and DLC-W coated discs showed fine-grained structure and relevant smoothness, with no visible surface voids, defects, or cracks. The measured values of the average roughness (Ra) and root mean square roughness (Rq) for the CrN/DLC were 8.51 nm and 10.7 nm, respectively, while for the DLC-W coating the values were (Ra) 12.7 nm (Rq) 16.1 nm, respectively. The surface of the coatings shows a nanocluster structure. The AFM results show that CrN/DLC has finer grains than DLC-W. The topography also shows that DLC-W possesses more pores than CrN/DLC.



**Figure 4.** AFM images: (a) CrN/DLC, (b) DLC-W.

### 3.1. Tribological Behavior of CrN/DLC and DLC-W Coating

#### 3.1.1. Coefficients of Friction and Wear Rates of Substrate and Coatings

The tribological behavior of uncoated, CrN/DLC, and DLC-W coated specimens were determined using the SRV Reciprocating test at 25 °C, 150 °C, 200 °C, and 250 °C. Figure 5a shows the average steady-state COF values at different temperatures (25 °C, 150 °C, 200 °C, and 250 °C). Significant fluctuations were observed for the uncoated carburized and hardened discs (substrate) at all temperatures. At elevated temperatures, most DLC coatings undergo permanent chemical and structural changes; hence, their friction and wear behavior degrades.

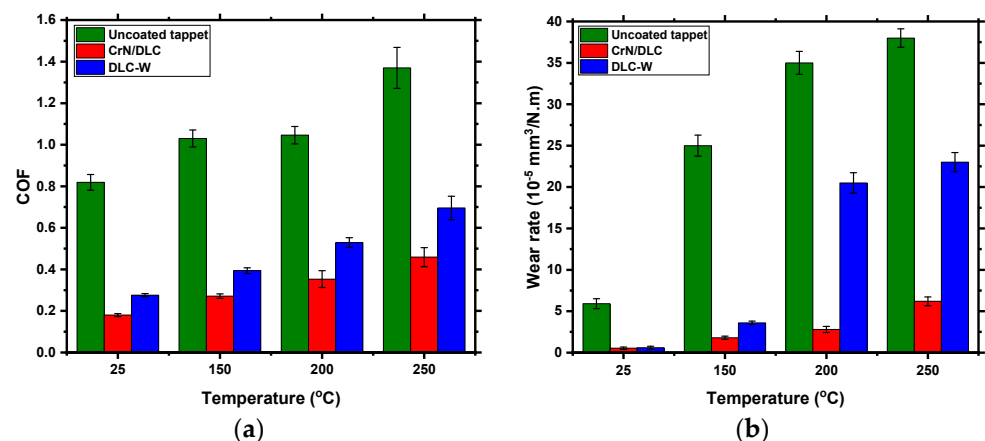


**Figure 5.** Uncoated and coated tappet valve tested against AISI 52,100 balls at 25, 150, 200, and 250 °C (a) average coefficient of friction; (b) specific wear rate.

Table 2 shows the COF and Wear Rate variations for the uncoated, CrN/DLC, and DLC-W coatings, with temperature.

**Table 2.** COF and wear rate variations for the uncoated, CrN/DLC, and DLC-W coatings, with temperature.

Coating	Uncoated		CrN/DLC		DLC-W	
Temperature	COF	Wear Rate (mm <sup>3</sup> /Nm)	COF	Wear Rate (mm <sup>3</sup> /Nm)	COF	Wear Rate (mm <sup>3</sup> /Nm)
25 °C	0.83	5.9 × 10 <sup>−5</sup>	0.18	0.5 × 10 <sup>−5</sup>	0.28	0.6 × 10 <sup>−5</sup>
150 °C	1.03	15.0 × 10 <sup>−5</sup>	0.27	1.8 × 10 <sup>−5</sup>	0.39	3.6 × 10 <sup>−5</sup>
200 °C	1.05	25.0 × 10 <sup>−5</sup>	0.35	2.8 × 10 <sup>−5</sup>	0.53	20.5 × 10 <sup>−5</sup>
250 °C	1.37	35.0 × 10 <sup>−5</sup>	0.47	6.2 × 10 <sup>−5</sup>	0.69	23.0 × 10 <sup>−5</sup>

Figure 5 shows the COFs and wear rate (Ws) variation of the uncoated, CrN/DLC, and DLC-W coated discs tested at 25 °C, 150 °C, 200 °C, and 250 °C. The wear rate was calculated using Equation (1).

One can see that COFs increase steadily with increasing temperature in uncoated, CrN-DLC coated, and DLC-W coated conditions. The uncoated specimens showed friction coefficients greater than unity when tested at temperatures 150 °C and higher, indicating the occurrence of adhesive wear. The COFs for both CrN/DLC and DLC-W were lower than the uncoated valve tappet at all temperatures, indicating an improvement of the substrate by the CrN/DLC and DLC-W coatings. The CrN/DLC COFs were much lower than the ones measured for the DLC-W at all temperatures.

The obtained results are in accordance with the trend shown in the paper by Becker et al. [24]. Aside from the improvement in the adhesion of the coating to the substrate by the use of Cr interlayers, the lower COFs obtained for the CrN/DLC may be assigned to a higher sp<sup>3</sup> content, which is responsible for a higher hardness (lower deformation, even up to 250 °C), compared to the sp<sup>3</sup> content and lower hardness of the DLC-W coating [25,26]. Topography results also corroborate the higher friction coefficients of the DLC-W coating due to more defects and greater grain size, implying a Ra value (12.7 nm) higher than DLC (8.51 nm).

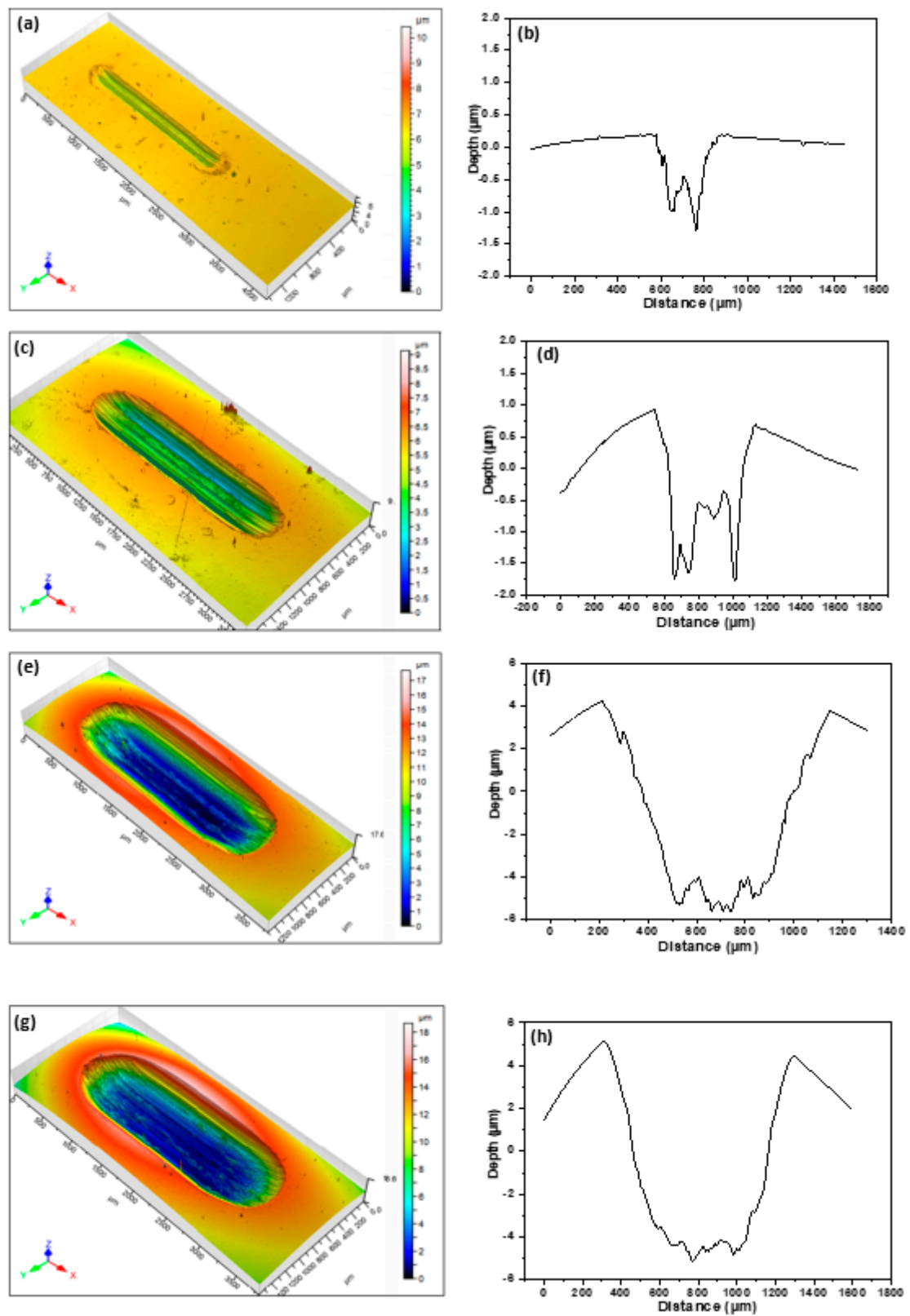
The higher fluctuation in the DLC-W can result from the alternating soft and hard sub-layers in the multilayer DLC-W. The results are also corroborated by those published in the literature [13,15,18,21,25–29].

The variation in the wear rates of the CrN/DLC and DLC-W coatings at 25 °C, 150 °C, 200 °C, and 250 °C shows a good correlation with the friction characteristics. It is worth noting that the increase in wear rates for both uncoated and coated discs with temperature follows the observed decrease in coating hardness. The wear rates and COFs obtained here are also similar to those reported in the literature [25,27].

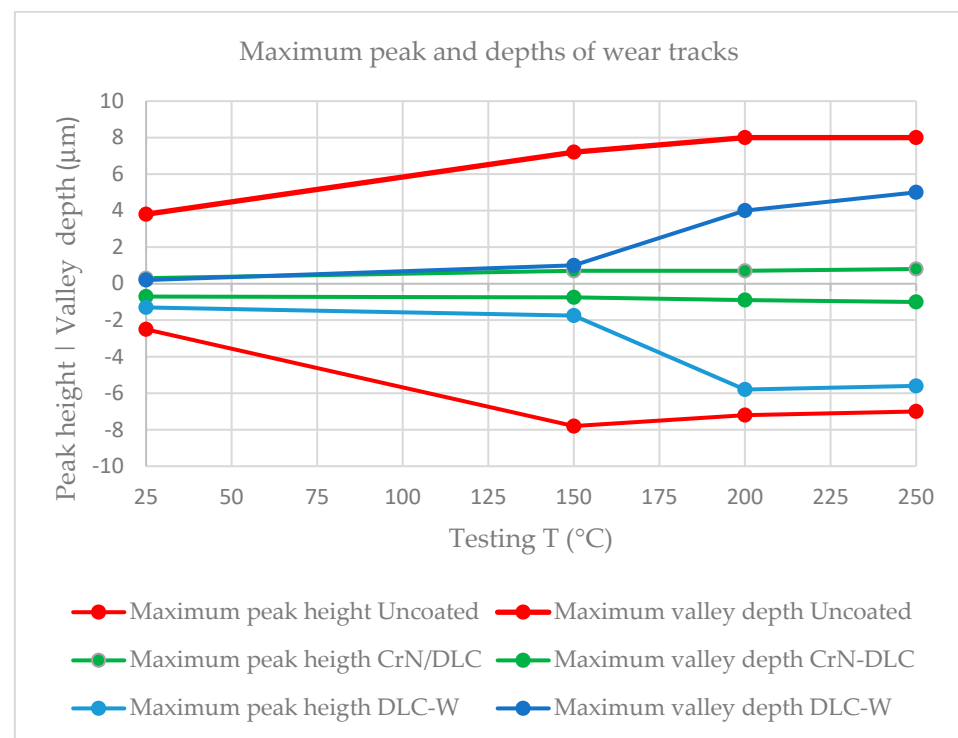
### 3.1.2. D Profilometry

Figure 6 shows an example of typical 3D and 2D images taken from the profilometry tests for the DLC-W coating at 25 °C, 150 °C, 200 °C, and 250 °C.

The maximum peak heights and minimum valley depths taken from the 3D and 2D profilometry tests of the uncoated, CrN/DLC, and DLC-W coated surfaces were assessed and plotted as graphs in Figure 7. When comparing the wear tracks' maximum peak height and lowest valley depth for the four tested temperatures, one can see that as the temperature increases, there is a corresponding increase in the depth and width of the wear track for both uncoated and coated discs. The CrN/DLC and DLC-W coatings showed a much better wear resistance than the uncoated samples. The DLC-W behaved reasonably well up to 150 °C but showed greater maximum peak and depths of the wear tracks at 200 °C and 250 °C.



**Figure 6.** 3D and 2D image of wear track for DLC-W coated tappet (a,b) 25 °C (c,d) 150 °C (e,f) 200 °C (g,h) 250 °C.



**Figure 7.** Maximum peak and depths of wear tracks for the uncoated, CrN/DLC coated, and DLC-W coated discs at 25 °C, 150 °C, 200 °C, and 250 °C, taken from the 3D and 2D profilometry images.

The DLC coatings show low friction and high wear resistance at ambient temperature due to the formation of graphitic tribolayer at the asperity contacts. At these regions,  $sp^3$  bonds transform into  $sp^2$  [21,30–32]. The wear rates continue to increase as the temperature increases due to an increase in the  $sp^2$  content in the CrN/DLC coatings, resulting in a softer coating that quickly wears out at higher temperatures. An increase in wear rate for DLC-W with tungsten is more likely due to the presence of WC nanoparticles acting as an abrasive component [30,33–35]. At 25 °C, the wear rate is slightly higher than CrN/DLC due to lower  $sp^3$  content, and as the temperature increases, the  $sp^2$  content continues to increase, reducing the DLC-W coating's hardness and wear resistance. Moreover, oxidation also begins to occur, and the removal of the coatings at 200 °C and 250 °C can be observed in the next section.

### 3.1.3. Wear Mechanisms and Surfaces Analysis at Various Temperature

To further investigate the friction and wear behaviors of the CrN/DLC and DLC-W coatings, the morphology of the wear tracks for the uncoated, CrN/DLC, and DLC-W coated valve tappet tested, and wear scars for the contact steel balls at 25 °C, 150 °C, 200 °C, and 250 °C were observed by SEM/EDS. The results are shown in Figures 8–15. The wear track of the uncoated valve tappet at 25 °C had adhered material and scratches aligned in the sliding direction of the contact ball, as seen in Figure 8a; this could result from mixed abrasion and adhesion wear mechanisms. EDS compositional analysis revealed that the adhered material of the uncoated valve tappet was rich in C, O, Fe, and a trace of Mn, which were contributions from both the valve tappet and contact ball see Figures 8a and 9a. The SEM image and EDS compositional analysis revealed that the contact ball had adhered materials of C-O, Fe-O, and N-O (Figure 10), responsible for the high friction and wear rates. The observations indicate that adhesive wear is predominant, in accordance with the observed friction coefficients greater than unity.



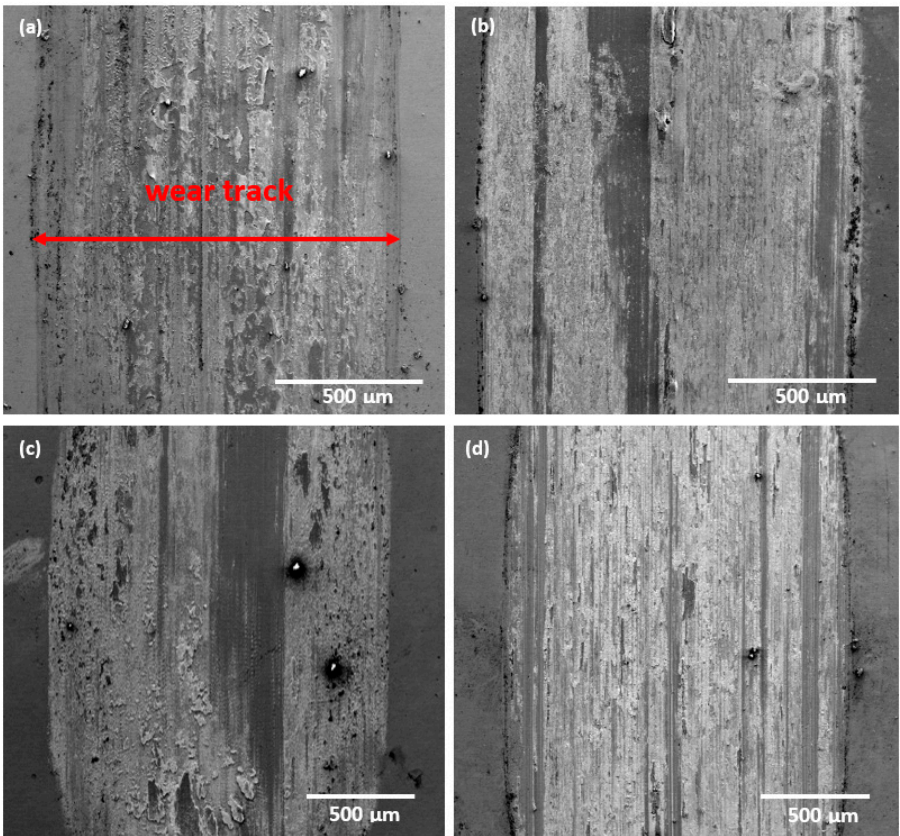


Figure 8. Wear tracks for uncoated tappets (a) 25 °C, (b) 150 °C, (c) 200 °C, (d) 250 °C.

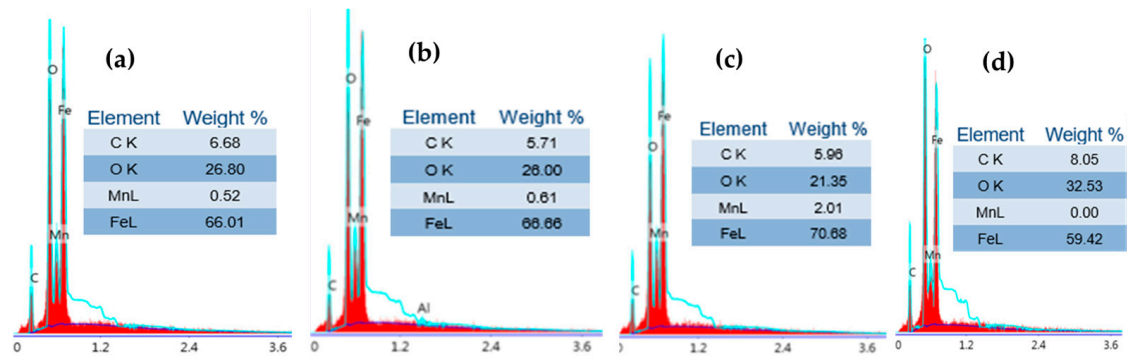


Figure 9. EDS analysis of the wear tracks for uncoated tappet (a) 25 °C, (b) 150 °C, (c) 200 °C, (d) 250 °C.

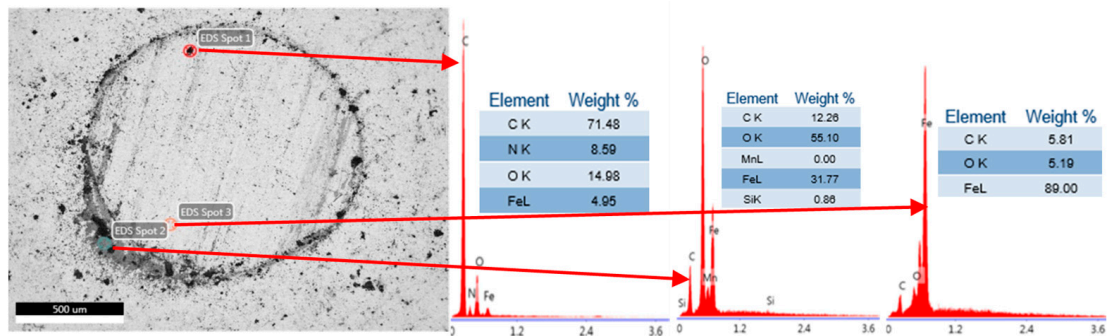
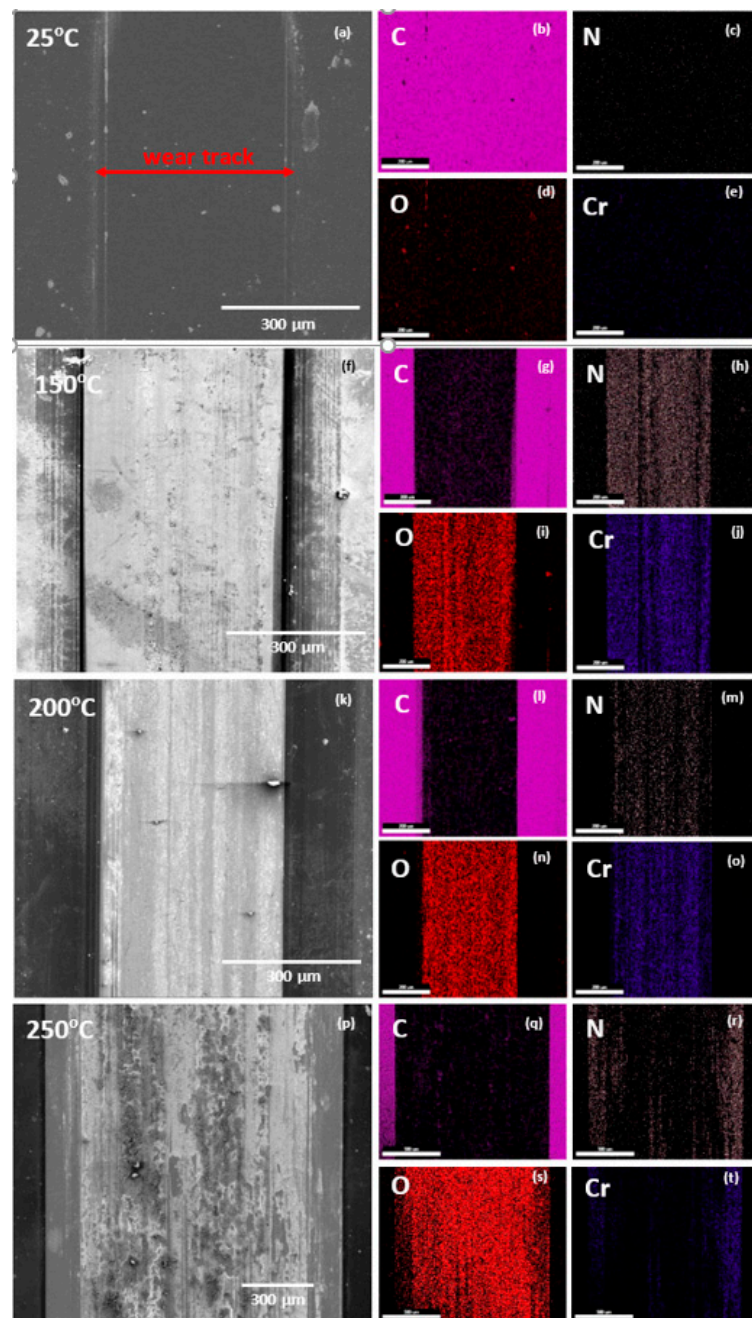
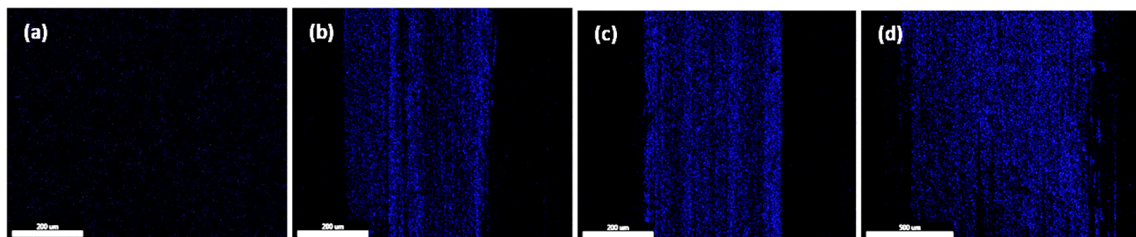


Figure 10. SEM image and EDS composition of wear scar for contact ball on uncoated tappet.



**Figure 11.** SEM images of wear track for CrN/DLC coated tappet at (a) 25 °C, (f) 150 °C, (k) 200 °C, (p) 250 °C. Elemental EDS mapping at 25 °C, (b) C, (c) N, (d) O, (e) Cr at 150 °C, (g) C, (h) N, (i) O, (j) Cr at 200 °C, (l) C, (m) N, (n) O, (o) Cr at 250 °C, (q) C, (r) N, (s) O, (t) Cr.



**Figure 12.** Elemental EDS mapping for Fe of wear track for CrN/DLC coated tappet at (a) 25 °C (b) 150 °C (c) 200 °C (d) 250 °C.



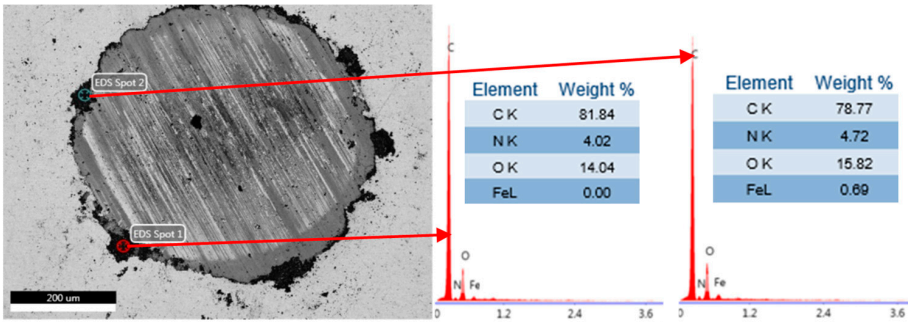


**Figure 13.** SEM image and EDS composition of wear scar for the contact ball on CrN/DLC coatings at 25 °C.

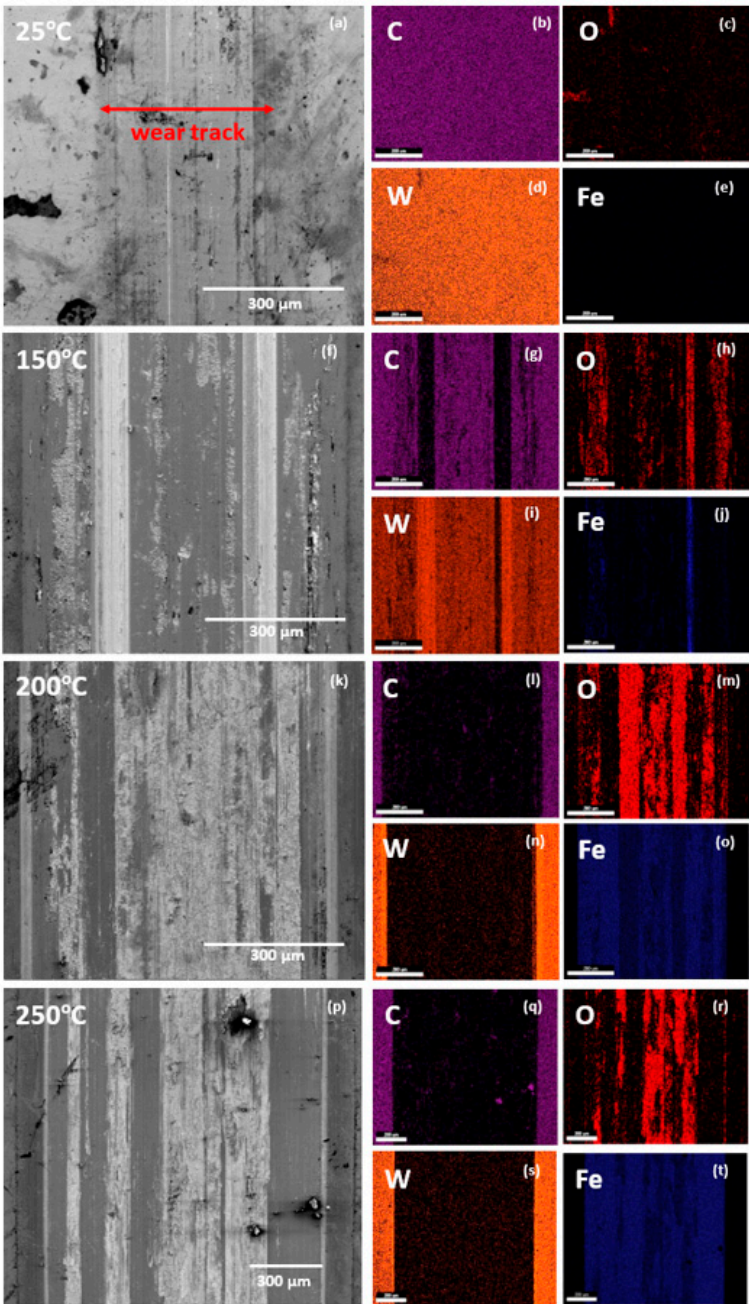


**Figure 14.** SEM images and EDS mapping of the wear track for DLC-W coated tappet at (a–e) 25 °C, (f–j) 150 °C, (k–o) 200 °C, (p–t) 250 °C.

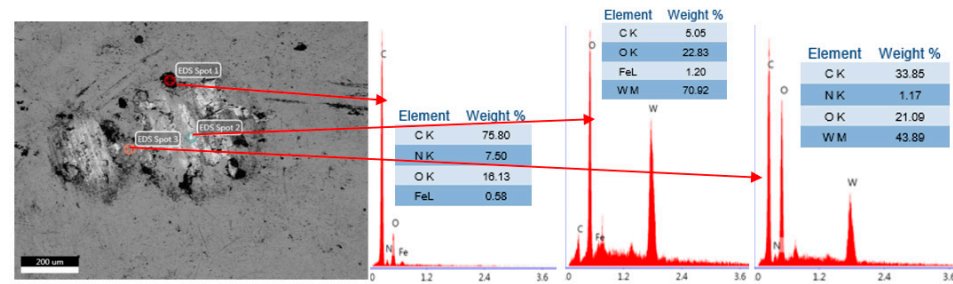


**Figure 15.** SEM image and EDS composition of wear scar for contact ball on DLC-W coatings.

The wear track of the CrN/DLC coating at 25 °C depicted adhered material, detached particles, and fine scratches aligned in the sliding direction of the contact ball, suggesting that the wear mechanisms were a mixture of abrasion and adhesion as can be seen in Figure 11a.

Accumulated materials removed from the coatings were observed at the end of the wear track. The corresponding EDS elemental mapping showed the distributions of the elements on the wear track, namely, Cr, O, N, and C, as seen in Figure 11b–e. However, Fe–O was absent at 25 °C in the wear track, as shown in Figure 12.

Figure 13 shows the SEM image of the contact ball and the EDS compositional analysis, which revealed that the contact ball surface comprises a mixture of high C-containing wear debris, together with N–O and Fe–O.

The O observed was due to oxidation during the contact ball's sliding on the coating's surface. C-rich particles observed on the contact ball from the coating reduced friction and wear at 25 °C.

The wear tracks of the DLC-W coating at 25 °C depict similar behavior as CrN/DLC coating at 25 °C, with wear mechanisms exhibiting a mix of abrasion and adhesion wear mechanisms consisting of adhered material, detached particles, and fine scratches aligned in the sliding direction of the contact ball as shown in Figure 14. The corresponding EDS elemental mapping showed the distributions of the elements on the wear track namely, W, O, Fe, and C as seen in Figure 14a–e.

Removed materials from the coatings were observed at the end of the wear track. The adhered materials on the contact ball, which were analyzed using EDS compositional analysis, suggest that the material was rich in C–O, Fe–O, N–O, W–C, and W–O Figure 15. It is worth noting that the oxides and graphitic particles are accumulated at the border of the contact surface, showing that the contact between body and counterbody is predominantly adhesive.

The C-rich and W-rich particles, and the presence of O, form abrasive particles can also be responsible for the slight increase in friction and wear rate compared to CrN/DLC coating.

Detached particles observed in the wear track could be a mixture of non-oxidized and oxidized particles from the coatings and the contact ball during sliding. Wear debris was found to adhere to the border region of the contact ball, which was similar to those on the wear track. At the protuberances of the contact, a local increase in temperature usually arises due to the friction generated by the sliding of the contact ball against the surface of the coatings. During the continuous sliding of the contact ball, asperities from both the ball and the coating surface usually break away, generating wear debris particles, which are oxidized and adhere to the surfaces. This continuous process leads to scratching of the surfaces and coating removal. Most of the wear debris was ejected from the wear track as the ball's movement continued.

A decrease in hardness (Table 2) caused by W addition made the material removal from the DLC-W coatings easier compared to CrN/DLC, which agrees with the increased wear rate observed in Figure 5b. The wear track was also observed to increase in width and depth for DLC-W compared to CrN/DLC coatings.

The test conducted at higher temperatures (150 °C, 200 °C, and 250 °C) had evidence of deformation at the edge of the wear tracks with deeper and wider wear tracks with fine

scratches in the sliding direction, suggesting predominantly adhesive wear as the active mechanism for the CrN/DLC and DLC-W coated discs, as shown in Figure 11f,k,p and Figure 14f,k,p respectively. Here, the wear scars on the contact ball had smoother and shallower scratches, and small oxidized wear debris was found to adhere to the wear scars as shown in Figures 13 and 15. In contrast, a very high amount of adhered material was observed at the surface of the uncoated and coated valve tappet formed by oxides. The wear track had rough and deeper scratches in the sliding direction due to mixed adhesion and abrasion mechanisms. The coatings oxidize spontaneously at these temperatures due to their low oxidation resistance [19].

The detection of Cr on the wear track of the CrN/DLC coating at 200 °C and 250 °C indicates that the DLC coating has been removed, leaving the CrN layer on the surface. EDS compositional analysis revealed that the contact ball surface comprised a mixture of high C-containing wear debris, N-O, Fe-O, and predominantly C-O (see Figure 13). Figure 11 agrees with the observed wear rate and COF.

More removed materials from the coatings were observed at the end of the track, exposing the substrate (valve tappet) partially at 200 °C and severely at 250 °C, as seen in Figure 14k,p. The presence of O was due to oxidation; a C-rich and W-rich transfer layer was observed on the contact ball from the coating, suggesting a rich WC layer, which was responsible for slightly increasing the COF and wear rate compared to CrN/DLC. Figure 14 also is in agreement with the wear rate and COF. An increase in hard WC1-x particles increases the COF and wear rate at 250 °C.

Since the CrN/DLC and DLC-W coated valve tappet is protected by the C-rich transfer layer (for CrN/DLC) and WC-rich transfer layer (for DLC-W), the wear in the contact ball is much lower at 25 °C and 150 °C, giving rise to narrower, and shallower wear tracks. The CrN/DLC coating showed the best wear resistance at all temperatures due to its enhanced oxidation resistance and increased hardness, as reported in previous work published elsewhere [18,25]. The DLC-W coatings, on the other side, showed poor wear resistance at 200 °C and 250 °C due to the presence of hard oxide particles, lower hardness, and greater roughness due to the presence of growth defects at the interface. The sliding contact between the adhered debris at the ball and the coating surface, from which the oxides are being removed, leads to similar COF, regardless of the composition of the films.

The combined oxides of iron and tungsten carbide contribute to the formation of a transition layer, causing a strong bonding of DLC-W onto the metallic substrate at 25 °C and 150 °C. However, as the temperature increases to 200 °C and 250 °C, there is an increase in the removal of WC, which fails to form transfer layers and becomes very hard [36], thereby increasing the abrasive wear at these temperatures and causing a rise in COF and wear. The analysis of friction that occurred suggests that the initial stage is dominated by graphitization accompanied by tribo-oxidation of the coating [30]. The DLC-W is easily consumed under mild conditions and low wear rates [37], so it performed slightly worse than the CrN/DLC coatings at 25 °C and 150 °C and severely worse at 200 °C and 250 °C.

#### Raman Analysis of the Wear Track

Further investigation of the wear track (inside and outside) of CrN/DLC and DLC-W at 25 °C, 150 °C, 200 °C, and 250 °C by Raman spectroscopy was carried out. The G and D peaks, G position, and ID/IG ratio were determined at 25 °C, 150 °C, 200 °C, and 250 °C. The results in Figure 16 show the G position ( $\text{cm}^{-1}$ ) and ID/IG ratio for inside and outside the wear track at different temperatures.

The result shows that for both CrN/DLC and DLC-W coatings, there were very few differences in the ID/IG and G Positions outside of the wear tracks, which may be due to the effect of small changes caused by the rise in temperature alone on the coatings, giving rise to a fluctuation in hardness and elastic modulus values at various temperatures and agrees with Figure 16. The ID/IG and G Positions inside the wear tracks showed significant changes for both CrN/DLC and DLC-W coatings, which could be due to the combined effect of temperature and plastic deformation taking place simultaneously on the surface of



the coatings. An increase in the ID/IG ratio and G Positions were observed for CrN/DLC and DLC-W coatings at 150 °C, 200 °C, and 250 °C. At 25 °C, the changes that occurred were small due to possible plastic deformation during the sliding of the contact ball on the coated valve tappet. In addition, the DLC-W coatings displayed a higher increase in ID/IG ratio and G Positions at various temperatures, implying a lower hardness and elastic modulus than CrN/DLC coatings at all temperatures.

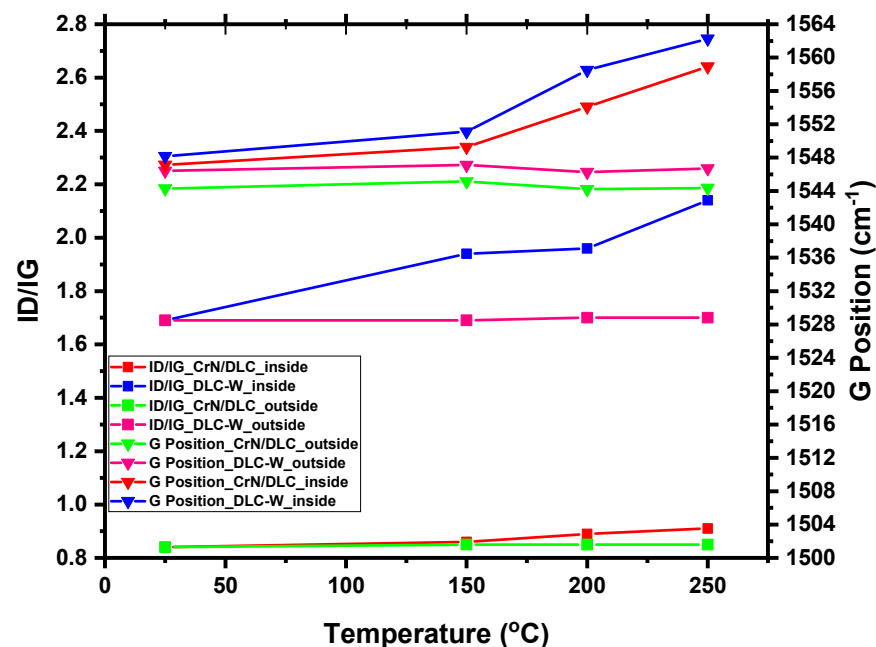


**Figure 16.** The effect of temperature on the ID/IG ratio and G Position for CrN/DLC and DLC-W coatings.

Furthermore, an additional peak at  $343\text{ cm}^{-1}$  [26] indicates the presence of iron oxide for the CrN/DLC, which is responsible for abrasive wear in the CrN/DLC coating. On the other hand, additional peaks at  $347\text{ cm}^{-1}$  and  $457\text{ cm}^{-1}$  [26] indicate the presence of tungsten oxide for the DLC-W coating. Sliding contact triggered the formation of a tungsten-oxide-rich layer, especially  $\text{WO}_3$  [26,36]. Therefore, the formation of tungsten oxide occurs when W particles become oxidized during the sliding process. In addition, the transfer layers containing graphitized carbon and lubricative  $\text{WO}_3$  are responsible for the low friction at 25 °C and 150 °C, with the graphitized carbon dominating at 25 °C and while  $\text{WO}_3$  dominates at higher temperatures (200 to 500 °C) [26,36].

#### Mechanical Properties of the Wear Track

The mechanical properties of the wear track were further investigated for CrN/DLC and DLC-W at various temperatures, as presented in Figures 17 and 18.

The hardness and elastic modulus inside and outside the wear track are presented. In addition, the  $\text{H}^3/\text{E}^2$  ratios inside and outside the wear track of the coatings at various temperatures were estimated. The material's  $\text{H}/\text{E}$  and  $\text{H}^3/\text{E}^2$  values reflect the elastic behavior and resistance to plastic deformation, respectively [38].

The higher  $\text{H}^3/\text{E}^2$  value of CrN/DLC indicates a better plastic deformation resistance. There was an insignificant change in the hardness, elastic modulus, and  $\text{H}^3/\text{E}^2$  for the outside of the wear track. Conversely, a reduction in the hardness value occurred inside the wear track due to deformation during sliding of the contact ball and transformation of  $\text{sp}^3$  to  $\text{sp}^2$  due to the increase in temperature. The hardness values continue to decrease as the temperature increases. In contrast, the elastic modulus increased to 200 °C and then decreased. The  $\text{H}^3/\text{E}^2$  ratio decreased drastically from 25 °C to 200 °C, then increased slightly to 250 °C. The change in mechanical properties for the CrN/DLC coatings at

different temperatures may be due to deformation, an increase in temperature, an increase in the number of C-rich transfer layers, and an increase in the contribution from the substrate. Therefore, a larger plastic strain is expected with a smaller H/E ratio. This implies that the coatings with a higher H/E ratio must possess smaller accumulative strain and strain energy, leading to better wear resistance [39,40].

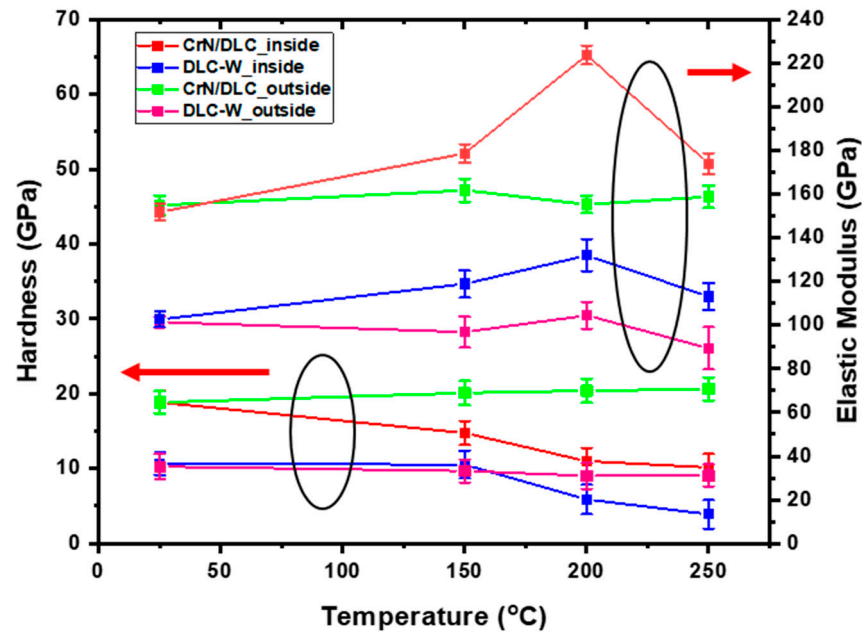


Figure 17. Hardness and elastic modulus at different temperatures for CrN/DLC and DLC-W coatings.

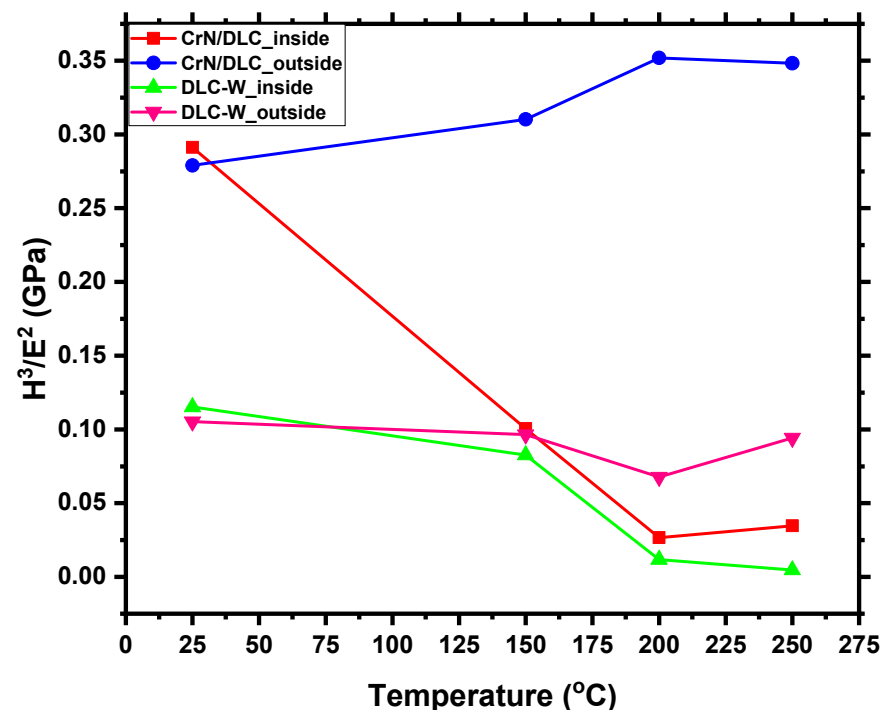


Figure 18.  $H^3/E^2$  at different CrN/DLC and DLC-W coatings temperatures.

On the other hand, for DLC-W coatings, the hardness value inside the wear track reduced rapidly from 25 °C to 250 °C, a consequence of deformation as the temperature increased, while the elastic modulus decreased to 150 °C, increased to 200 °C and finally

decreased to 250 °C and  $H^3/E^2$  ratio decreased drastically from 25 °C to 200 °C, and then increased slightly up to 250 °C.

#### 4. Conclusions

The experimental work carried out in this investigation did not intend to reproduce or mimic the operating conditions of the tribological pair camshaft/cam follower in a valve train. Instead, uncoated, CrN/DLC, and DLC-W coated carburized and hardened 16 MnCr5 steel discs were submitted to SRV linear reciprocating testing in non-lubricated contact against a hardened 60 HRC 52,100 sphere in much more severe conditions. The effect of intermediate testing temperatures below 300 °C on the friction coefficients and wear rates was explored. For the experimental conditions of the work done, it was possible to draw the following conclusions:

- The CrN/DLC coating showed the lowest wear rates during the sliding reciprocating tests at 25 °C. Increasing the testing temperature leads to an increase in friction coefficient. However, CrN/DLC COFs remained the lowest compared to DLC-W and uncoated valve tappet at all temperatures.
- The DLC-W coating showed low wear rates at 25 °C and 150 °C. However, at 200 °C and 250 °C, the wear rate strongly increased due to the total removal of the coatings from the substrate, thereby exposing the tappet valve to direct contact with the sliding ball.
- The uncoated valve tappet showed the highest wear rate at all temperatures and increased significantly with increasing temperature.
- The results revealed that deposition of CrN/DLC and DLC-W improved the tribological performance of the discs at all temperatures.
- The structural and mechanical properties of both CrN/DLC and DLC-W coatings reduced as the temperature increased.
- The use of a multilayer DLC-W coating for tribological applications at elevated temperatures is unsuitable because it was quickly consumed, even during SRV testing at 150 °C.

**Author Contributions:** Conceptualization, F.O.K., S.K.K., N.K.F., R.M.d.S., A.P.T.; methodology, N.K.F., L.B.V., P.K.V., R.M.d.S., A.P.T.; investigation F.O.K., S.K.K., N.K.F., L.B.V., P.K.V., R.M.d.S., A.P.T.; resources, P.K.V., D.A.L., R.M.d.S., A.P.T.; writing—original draft preparation, F.O.K.; writing—review and editing, F.O.K., A.P.T.; supervision, A.P.T.; project administration, A.P.T.; funding acquisition, N.K.F., R.M.d.S., A.P.T. All authors have read and agreed to the published version of the manuscript.

**Funding:** The APC was funded by Fundação de Apoio à Universidade de São Paulo (project 065). The Petroleum Technology Development Funds (PTDF) (contract w/No), Nigeria and Conselho Nacional de Desenvolvimento Científico e Tecnológico (CNPq)—Brazil process 141991/2019-4 for financial support. A.P.Tschiptschin acknowledges the financial support of FAPESP Thematic Project 2019/18572-7.

**Institutional Review Board Statement:** Not applicable.

**Informed Consent Statement:** Not applicable.

**Data Availability Statement:** Data are contained within the article.

**Acknowledgments:** The authors are grateful to HEF Durferrit, Brazil for the deposition of the coatings. F.O. Kolawole acknowledges Marcos D. Santos and Arnaldo O. Lima of the Surface Phenomena Laboratory (LFS), for the nanoindentation, Raman measurements and 3D Profilometry and Maria Cecilia Salvadori and Fernanda de Sá Teixeira of the Physics Institute—USP, for the AFM measurements.

**Conflicts of Interest:** The authors declare no conflicts of interest. The funders had no role in the design of the study; in the collection, analyses, or interpretation of data; in the writing of the manuscript; or in the decision to publish the results.

## References

- Holmberg, K.; Andersson, P.; Erdemir, A. Global energy consumption due to friction in passenger cars. *Tribol. Int.* **2012**, *47*, 221–234. [\[CrossRef\]](#)
- Erdemir, A.; Fenske, G.R. Tribological performance of diamond and diamond-like carbon films at elevated temperatures. *Tribol. Trans.* **1996**, *39*, 787–794. [\[CrossRef\]](#)
- Erdemir, A.; Donnet, C. Tribology of diamond-like carbon films: Recent progress and future prospects. *J. Phys. D Appl. Phys.* **2006**, *39*, 18. [\[CrossRef\]](#)
- Robertson, J. Diamond-like amorphous carbon. *Mater. Sci. Eng. R Rep.* **2002**, *37*, 129–281. [\[CrossRef\]](#)
- Dearnley, P.A.; Neville, A.; Turner, S.; Scheibe, H.J.; Tietema, R.; Tap, R.; Stuber, M.; Hovsepian, P.; Layyous, A.; Stenbom, B. Coatings tribology drivers for high density plasma technologies. *Surf. Eng.* **2010**, *26*, 80–96. [\[CrossRef\]](#)
- Kolawole, F.O.; Kolade, O.S.; Bello, S.A.; Kolawole, S.K.; Ayeni, A.T.; Elijah, T.F.; Borisade, S.G.; Tschiptschin, A.P. The improvement of diamond-like carbon coatings for tribological and tribo-corrosion applications in automobile engines: An updated review study. *Int. J. Adv. Manuf. Technol.* **2023**, *126*, 2295–2322. [\[CrossRef\]](#)
- Kolawole, F.O. Mechanical and Temperature-Dependent Tribological Behavior of CrN/DLC and Multilayer DLC-W Coatings for Automobile Engine Applications. Ph.D. Thesis, University of Sao Paulo, São Paulo, Brazil, November 2022.
- Kolawole, F.O.; Varela, L.B.; Kolawole, S.K.; Ramirez, M.A.; Tschiptschin, A.P. Deposition and characterization of tungsten oxide (WO<sub>3</sub>) nanoparticles incorporated diamond-like carbon coatings using pulsed-DC PECVD. *Mater. Lett.* **2021**, *282*, 1–4. [\[CrossRef\]](#)
- Kolawole, F.O.; Ramirez, M.A.; Kolawole, S.K.; Varela, L.B.; Tschiptschin, A.P. Deposition and characterization of molybdenum oxide (MoO<sub>3</sub>) nanoparticles incorporated diamond-like carbon coatings using pulsed-DC PECVD. *Mater. Lett.* **2020**, *278*, 1–4. [\[CrossRef\]](#)
- Borges, C.F.M.; Pfender, E.; Heberlein, J. Influence of nitrided and carbonitrided interlayers on enhanced nucleation of diamond on stainless steel 304. *Diam. Relat. Mater.* **2021**, *10*, 1983–1990. [\[CrossRef\]](#)
- Abdullah, T.H.; Wakayama, M.; Tokoroyama, T.; Kousaka, H.; Umehara, N.; Mabuchi, Y.; Higuchi, T. The effect of oil temperature and additive concentration on the wear of non-hydrogenated DLC coating. *Tribol. Int.* **2014**, *77*, 65–71. [\[CrossRef\]](#)
- Podgornik, B.; Jacobson, S.; Hogmark, S. DLC coating of boundary lubricated components—Advantages of coating one of the contact surfaces rather than both or none. *Tribol. Int.* **2003**, *36*, 843–849. [\[CrossRef\]](#)
- Bujak, J.; Michalczewski, R. Characterization and properties of low-friction, multilayered Cr-doped diamond-like carbon coatings prepared by pulse biased filtered cathodic arc deposition. *Pr°C. Inst. Mech. Eng. Part J J. Eng. Tribol.* **2011**, *225*, 875–882. [\[CrossRef\]](#)
- Lukaszewicz, K.; Paradecka, A.; Wiśniewska, J. Structure and properties of CrN/DLC coating deposited by PVD ARC-cathodes and PACVD technology. *Arch. Mater. Sci. Eng.* **2013**, *64*, 40–44.
- Mulligan, C.P.; Senick, M.; Schmidt, D.P.; Khominich, V.; Gay, Z.; Bell, D. CrN, CrN/SiC, and CrN/DLC coatings deposited by a novel arc plasma acceleration process: Process and properties. *Mater. Manuf. Process.* **2014**, *29*, 1037–1043. [\[CrossRef\]](#)
- Conde, F.F.; Ávila Diaz, J.A.; Da Silva, G.F.; Tschiptschin, A.P. Dependence of wear and mechanical behavior of nitroCarburized/CrN/DLC layer on film thickness. *Mater. Res.* **2019**, *22*, 1–10. [\[CrossRef\]](#)
- Mobarak, H.M.; Chowdhury, M. Tribological performance of hydrogenated amorphous carbon (a-C: H) DLC coating when lubricated with biodegradable vegetal canola oil. *Tribol. Ind.* **2014**, *36*, 163–171.
- Nakao, S.; Kimura, T.; Suyama, T.; Azuma, K. Conductive diamond-like carbon films prepared by high power pulsed magnetron sputtering with bipolar type plasma based ion implantation system. *Diam. Relat. Mater.* **2017**, *77*, 122–130. [\[CrossRef\]](#)
- Evaristo, M.; Fernandes, F.; Cavaleiro, A. Room and High Temperature Tribological Behaviour of W-DLC Coatings Produced by DCMS and Hybrid DCMS-HiPIMS Configuration. *Coatings* **2020**, *10*, 319. [\[CrossRef\]](#)
- Takeno, T.; Miki, H.; Sugawara, T.; Hoshi, Y.; Takagi, T. A DLC/W-DLC multilayered structure for strain sensing applications. *Diam. Relat. Mater.* **2008**, *17*, 713–716. [\[CrossRef\]](#)
- Takeno, T.; Komiyama, T.; Miki, H.; Takagi, T.; Aoyama, T. XPS and TEM study of W-DLC/DLC double-layered film. *Thin Solid Films* **2009**, *517*, 5010–5013. [\[CrossRef\]](#)
- Bai, M.; Yang, L.; Li, J.; Luo, L.; Sun, S.; Inkson, B. Mechanical and tribological properties of Si and W doped diamond like carbon (DLC) under dry Reciprocating sliding conditions. *Wear* **2021**, *484–485*, 204046. [\[CrossRef\]](#)
- Kolawole, F.O.; Santos, M.D.; Kolawole, S.K.; Vencovsky, P.K.; Ludewigs, D.A.; Tschiptschin, A.P. Nano-Scratch and Micro-Scratch Properties of CrN/DLC and DLC-W Coatings. *Mater. Perform. Charact.* **2023**, *12*, 320–340. [\[CrossRef\]](#)
- Becker, J.; Colas, M.; Gies, A.; Hessel, S.; Karner, H.; Seibert, F.; Stelzig, T. Thermal effects influencing stability and performance of coatings in automotive applications. *Surf. Coat. Technol.* **2015**, *284*, 166–172. [\[CrossRef\]](#)
- Liu, Z.; Yue, W.; Wang, S.; Fu, Z.; Wang, C.; Liu, J. Preparation and Characterization of Sulfurized Tungsten Doped Non-hydrogenated Diamond-Like Carbon Films. *Plasma Chem. Plasma Process.* **2015**, *35*, 769–783. [\[CrossRef\]](#)
- Banerji, A.; Bhowmick, S.; Alpas, A.T. High temperature tribological behavior of W containing diamond-like carbon (DLC) coating against titanium alloys. *Surf. Coat. Technol.* **2014**, *241*, 93–104. [\[CrossRef\]](#)
- Le Huu, T.; Zaidi, H.; Paulmier, D.; Voumard, P. Transformation of sp<sup>3</sup> to sp<sup>2</sup> sites of diamond like carbon coatings during friction in vacuum and under water vapour environment. *Thin Solid Film* **1996**, *290–291*, 126–130. [\[CrossRef\]](#)
- Bhowmick, S.; Banerji, A.; Alpas, A.T. Tribological behaviour of W-DLC against an aluminium alloy subjected to lubricated sliding. *Tribol. Ind.* **2015**, *37*, 277–283.

29. Cao, L.; Liu, J.; Wan, Y.; Pu, J. Corrosion and trib<sup>o</sup>Corrosion behavior of W doped DLC coating in artificial seawater. *Diam. Relat. Mater.* **2020**, *109*, 108019. [[CrossRef](#)]
30. Czyzniewski, A.; Gulbinski, W.; Radnóczy, G.; Szerencsi, M.; Pancielejko, M. Microstructure and mechanical properties of W-C:H coatings deposited by pulsed reactive magnetron sputtering. *Surf. Coat. Technol.* **2011**, *205*, 4471–4479. [[CrossRef](#)]
31. Hovsepian, P.E.; Mandal, P.; Ehiasarian, A.P.; Sáfrán, G.; Tietema, R.; Doerwald, D. Friction and wear behaviour of Mo-W doped carbon-based coating during boundary lubricated sliding. *Appl. Surf. Sci.* **2016**, *366*, 260–274. [[CrossRef](#)]
32. Takeno, T.; Sugawara, T.; Miki, H.; Takagi, T. Deposition of DLC film with adhesive W-DLC layer on stainless steel and its tribological properties. *Diam. Relat. Mater.* **2009**, *18*, 1023–1027. [[CrossRef](#)]
33. Arslan, A.; Masjuki, H.H.; Quazi, M.M.; Kalam, M.A.; Varman, M.; Jamshaid, M.; Ashrafur Rahman, S.M.; Imran, M.; Zulfattah, Z.M.; Anwar, M.T.; et al. Experimental investigation of tribological properties of laser textured tungsten doped diamond like carbon coating under dry sliding conditions at various loads. *Mater. Res. Express.* **2019**, *6*, 106444. [[CrossRef](#)]
34. Müller, I.C.; Sharp, J.; Rainforth, W.M.; Hovsepian, P.; Ehiasarian, A. Tribological response and characterization of Mo–W doped DLC coating. *Wear* **2017**, *376–377*, 1622–1629. [[CrossRef](#)]
35. Konca, E.; Cheng, Y.T.; Weiner, A.M.; Dasch, J.M.; Alpas, A.T. Elevated temperature tribological behavior of non-hydrogenated diamond-like carbon coatings against 319 aluminum alloy. *Surf. Coat. Technol.* **2006**, *200*, 3996–4005. [[CrossRef](#)]
36. Pu, J.; He, D.; Wang, L. Effects of WC phase contents on the microstructure, mechanical properties and tribological behaviors of WC/a-C superlattice coatings. *Appl. Surf. Sci.* **2015**, *357*, 2039–2047. [[CrossRef](#)]
37. Cavaleiro, A.; De Hosson, J.T.M. *Nanostructured Coatings*; Springer Publishing: New York, NY, USA, 2006.
38. Yang, F.; Yang, S.Y.; Chang, X.X.; Yang, W.F.; Song, R.G.; Zheng, X.H. Microstructure and properties of DLC/CNx films with different CNx sublayer thicknesses. *Surf. Coat. Technol.* **2019**, *374*, 418–423. [[CrossRef](#)]
39. Guha, S.; Das, S.; Bandyopadhyay, A.; Das, S.; Swain, B.P. Investigation of mechanical properties of CVD grown titanium silicon nitride thin films under reduced atmosphere. *Appl. Phys. A* **2018**, *124*, 1–8. [[CrossRef](#)]
40. Leyland, A.; Matthews, A. On the significance of the H/E ratio in wear control: A nanocomposite coating approach to optimised tribological behaviour. *Wear* **2000**, *246*, 1–11. [[CrossRef](#)]

**Disclaimer/Publisher’s Note:** The statements, opinions and data contained in all publications are solely those of the individual author(s) and contributor(s) and not of MDPI and/or the editor(s). MDPI and/or the editor(s) disclaim responsibility for any injury to people or property resulting from any ideas, methods, instructions or products referred to in the content.